World Academy of Science, Engineering and Technology
International Journal of Mechanical and Mechatronics Engineering
Vol:9, No:5, 2015

Numerical Analysis of Laminar Reflux Condensation from Gas-Vapour Mixtures in Vertical Parallel Plate Channels

Foad Hassaninejadafarahani, Scott Ormiston

Abstract—Reflux condensation occurs in vertical channels and tubes when there is an upward core flow of vapour (or gas-vapour mixture) and a downward flow of the liquid film. The understanding of this condensation configuration is crucial in the design of reflux condensers, distillation columns, and in loss-of-coolant safety analyses in nuclear power plant steam generators. The unique feature of this flow is the upward flow of the vapour-gas mixture (or pure vapour) that retards the liquid flow via shear at the liquid-mixture interface. The present model solves the full, elliptic governing equations in both the film and the gas-vapour core flow. The computational mesh is non-orthogonal and adapts dynamically the phase interface, thus produces a sharp and accurate interface. Shear forces and heat and mass transfer at the interface are accounted for fundamentally. This modeling is a big step ahead of current capabilities by removing the limitations of previous reflux condensation models which inherently cannot account for the detailed local balances of shear, mass, and heat transfer at the interface. Discretisation has been done based on finite volume method and co-located variable storage scheme. An in-house computer code was developed to implement the numerical solution scheme. Detailed results are presented for laminar reflux condensation from steam-air mixtures flowing in vertical parallel plate channels. The results include velocity and gas mass fraction profiles, as well as axial variations of film thickness.

Keywords—Reflux Condensation, Heat Transfer, Channel, Laminar Flow.

I. Introduction

CONDENSATION in transport phenomena releases a significant amount of energy even for a small temperature difference due to the large difference between the liquid and vapour internal energies. Therefore, condensation heat transfer can be an important process in industrial applications and thermal systems.

A. Reflux Condensation

Reflux condensation can occur in vertical or inclined tubes or channels. The unique feature of reflux condensation is the upward flow of the gas-vapour mixture (or pure vapour) that retards the liquid flow via shear at the liquid-mixture (or liquid-vapour) interface. With sufficiently high vapour velocity and small channel height, the liquid can be held up by the mixture and completely close off the channel to vapour flow; this phenomenon is called flooding or inverted-slug flow. It represents a serious limitation to the operation of reflux condensers and much attention has been placed on determining the onset of flooding [1]. The motion of the liquid film is governed by the gravitational driving force and retarding force from the interfacial shear. At a particular mixture mass flow rate, the film velocity at the interface becomes zero. In this situation, the interfacial shear and gravitational force are equal. For the higher mixture mass flow rates, flow reversal occurs in the liquid film. Finally, the interfacial shear becomes dominant and the system reaches the total flooding limit.

Reflux condensation is one of the major heat removal mechanisms in loss of coolant safety analyses in nuclear power plant steam generators. In the system of pressurized water reactor and a steam generator, reflux condensation is expected to occur in the hot leg or U-tube during accidents caused by loss of coolant or by loss of heat removal in the mid-loop operation [2]. These accident scenarios occurred in pressurized water reactor plants in the USA in 1987 and 1990 [3].

Reflux condensation also can be observed in thermosyphons and heat pipes [4]. Thermosyphons transfer heat in the same way as heat pipes by the use of evaporation and condensation phenomena. In thermosyphons, there is no external equipment for the liquid transport from the condenser back to the evaporator and thus the evaporator must be located vertically below the condenser. Gravity is responsible for returning the condensate to the evaporator. Sometimes, thermosyphons are called gravity-assisted heat pipes.

Majority of previous modeling approaches for reflux condensation have been based on similar approximate governing equations and correlations at the interface. Most of them solved the equations for the liquid region and used correlations or simplified equations for the interface and mixture region. In addition, many of them did not consider gas in the mixture region and assumed pure vapour and they considered tubes and not channels [5]–[10].

One detailed study of reflux condensation simulation in tubes is that by Liao *et al.* [11]. They developed a heat and mass transfer analogy model for local heat transfer in reflux condensation of flowing vapour and non-condensable gases and compared the theoretical heat transfer with experiments. In their work, a liquid film model was derived from the two-phase integral momentum equation under counter-current flow condition. However, the inertial force terms in the momentum equation were neglected. In addition, it was assumed that the temperature profile is linear in the liquid region and longitudinal pressure gradient is equal in the gas and liquid regions. They calculated the film thickness based on

F. Hassaninejadafarahani and S. Ormiston are with the Department of Mechancial Engineering, University of Manitoba, Winnipeg, MB, Canada, (e-mail: hfarahani@umanitoba.ca).

the Reynolds number of the film and used a parabolic liquid velocity profile. For the gas phase, they used the heat and mass transfer analogy approach employing a diffusion layer model by Liao and Vierow [12] and applied a correlation to evaluate the friction factor at the interface for counter-current flow. An iterative marching scheme was used based on the assumption of an initial value for outlet vapour mass flow rate and interface temperature. Liao *et al.* predicted the heat transfer coefficients along the tube for a wide variety of turbulent reflux condensation conditions. Furthermore, they compared co-current and counter-current condensation and showed that the local condensate film behaviour should be treated differently between these two cases. They proposed that the condensate hydrodynamics is coupled to the gas motion and vapour condensation which are different for these two cases.

Finally, an understanding of reflux condensation is crucial in the design of reflux condensers and distillation columns. In distillation columns, for example, counter-current flow is used to separate components in mixtures of vapours that condense at different temperatures. To the best of authors' knowledge, there are no previous work on the computational modelling of reflux condensation in a vertical channel. Furthermore, the available open source and commercial software programs have limited capabilities in modeling this phenomenon.

The present work focuses on reflux condensation in vertical parallel plate channels and solves the fully coupled elliptic two-dimensional set of governing equations on a structured non-orthogonal grid including the mass, momentum, energy and gas mass fraction conservation equations. An Eulerian approach is used for the solution of the field variables. The mesh is implemented, however, so that a grid line always matches exactly with the liquid-mixture interface. At each time step, the interface location is updated and the mesh is re-generated. The solution for the field variables obtained using this new mesh. This iterative scheme, described in detail later, could be considered an adaptive Eulerian approach.

The sample results of present work will start to help to understand appropriate set of equations, boundary conditions and computational scheme for the simulation of reflux condensation from gas-vapour mixtures in vertical channels.

II. Mathematical Model

The main objective of this work is to develop a numerical model for reflux condensation in a vertical channel. The fundamental setup of condensation in vertical channel has a cooled section where the wall temperature (T_{wall}) is below the saturation temperature of the vapour. Due to the temperature difference between the mixture and wall, the vapour starts condensing on the channel wall and forms a thin film of condensate with the thickness of δ. The film thickness increases along the channel and the condensate flows downward as long as the summation of shear stress at the wall and at the interface is smaller than the gravitational force. As the mixture flows upward, the condensation rate decreases due to the interface temperature decrease and gas mass fraction increase. Finally, the condensation will stop and single phase mixture will exit the channel at the top.

The geometry of the vertical channel is shown in Fig. 1. In Fig. 1, the cooled section is the section with length of L_2 and constant wall temperature. Above and below the cooling section, boundary conditions must be specified for the mixture flow. The conditions of the mixture flow entering the channel from below are dependent on the geometry and thermal conditions in the piping that supplies the mixture. Taking this into account would extend the solution domain to include a three-dimensional region that is application-specific. Because developing a two-phase counter-current flow model will be a challenge itself, a two-dimensional model is considered an excellent starting point. Therefore, in order to keep the model domain two-dimensional and reasonable in size, an inlet section with an adiabatic wall with length of L_3 is added at the mixture inlet side of the cooled section. This additional length permits the development of the mixture flow before the cooled section and section of film flow with no mass flow change. Likewise, a section with an adiabatic wall of length L_1 is added at the mixture outlet side of the cooled section. This additional section permits the application of an appropriate outflow condition on the mixture as it flows without mass removal.

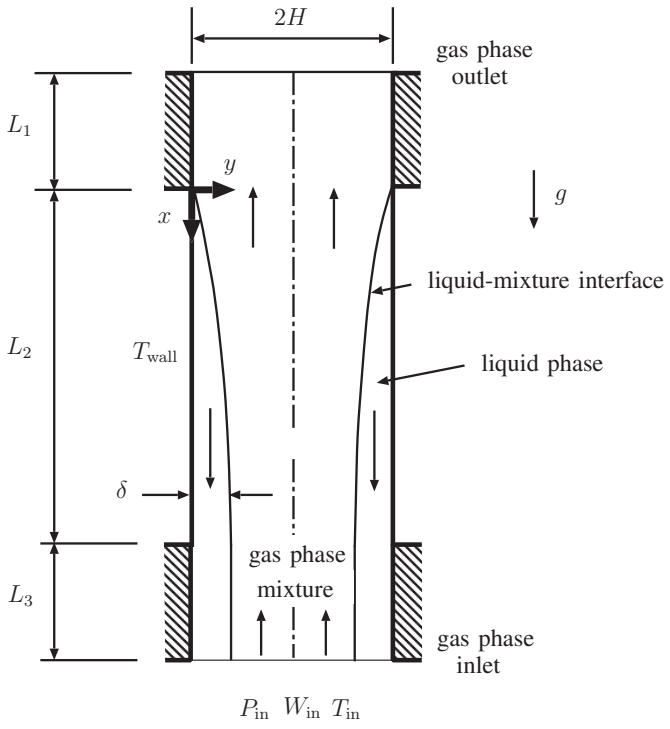

Fig. 1 Reflux condensation-model domain

A mixture of saturated vapour and air (as a non-condensable gas) flows in a vertical, parallel plate channel. The space between two plates is $2H$. The flow is two-dimensional and symmetrical about the centre line of the channel. The mixture has uniform profiles of pressure, temperature and gas mass fraction (P_{in}, T_{in} and W_{in}) at the gas phase inlet. To form the mathematical model, it was assumed that the flow is steady and laminar in both the liquid and mixture regions; that both liquid and mixture are Newtonian fluids; that the liquid-mixture

interface is smooth; that the vapour-gas mixture is an ideal gas mixture; that the vapour and gas have the same values of U, V and T in any location in the mixture. In addition, the saturation conditions were assumed at the liquid-mixture interface. The governing equations are written in Cartesian coordinates.

Equations (1), (2), (3) and (4) are the conservation of mass, x-momentum, y-momentum, and energy in the liquid region, respectively.

$$\frac{\partial}{\partial t}(\rho_L) + \frac{\partial}{\partial x}(\rho_L\ U_L) + \frac{\partial}{\partial y}(\rho_L\ V_L) = 0 \tag{1}$$

$$\frac{\partial\,(\rho_L\ U_L)}{\partial t} + \frac{\partial}{\partial x}(\rho_L\ U_L\ U_L) + \frac{\partial}{\partial y}(\rho_L\ V_L\ U_L) = -\frac{\partial P_L}{\partial x} + \frac{\partial}{\partial x}\left(\mu_L\ \frac{\partial U_L}{\partial x}\right) + \frac{\partial}{\partial y}\left(\mu_L \frac{\partial U_L}{\partial y}\right) + \rho_L\ g \tag{2}$$

$$\frac{\partial\,(\rho_L\ V_L)}{\partial t} + \frac{\partial}{\partial x}(\rho_L\ U_L\ V_L) + \frac{\partial}{\partial y}(\rho_L\ V_L\ V_L) = -\frac{\partial P_L}{\partial y} + \frac{\partial}{\partial x}\left(\mu_L \frac{\partial V_L}{\partial x}\right) + \frac{\partial}{\partial y}\left(\mu_L \frac{\partial V_L}{\partial y}\right) \tag{3}$$

$$\frac{\partial\left(\rho_L C_{p_L}\ T_L\right)}{\partial t} + \frac{\partial\left(\rho C_{p_L}\ U_L\ T_L\right)}{\partial x} + \frac{\partial\left(\rho_L C_{p_L}\ V_L\ T_L\right)}{\partial y} = \frac{\partial}{\partial x}\left(k_L \frac{\partial T_L}{\partial x}\right) + \frac{\partial}{\partial y}\left(k_L \frac{\partial T_L}{\partial y}\right) \tag{4}$$

In the mixture region, the governing equations are written as follows.

$$\frac{\partial}{\partial t}(\rho_M) + \frac{\partial}{\partial x}(\rho_M\ U_M) + \frac{\partial}{\partial y}(\rho_M\ V_M) = 0 \tag{5}$$

$$\frac{\partial\,(\rho_M\ U_M)}{\partial t} + \frac{\partial}{\partial x}(\rho_M\ U_M\ U_M) + \frac{\partial}{\partial y}(\rho_M\ V_M\ U_M) = -\frac{\partial P_M}{\partial x} + \frac{\partial}{\partial x}\left(\mu_M\ \frac{\partial U_M}{\partial x}\right) + \frac{\partial}{\partial y}\left(\mu_M \frac{\partial U_M}{\partial y}\right) + \rho_M\ g \tag{6}$$

$$\frac{\partial\,(\rho_M\ V_M)}{\partial t} + \frac{\partial}{\partial x}(\rho_M\ U_M\ V_M) + \frac{\partial}{\partial y}(\rho_M\ V_M\ V_M) = -\frac{\partial P_M}{\partial y} + \frac{\partial}{\partial x}\left(\mu_M \frac{\partial V_M}{\partial x}\right) + \frac{\partial}{\partial y}\left(\mu_M \frac{\partial V_M}{\partial y}\right) \tag{7}$$

$$\frac{\partial\left(\rho_M C_{p_M}\ T_M\right)}{\partial t} + \frac{\partial\left(\rho_M C_{p_M}\ U_M\ T_M\right)}{\partial x} + \frac{\partial\left(\rho_M C_{p_M}\ V_M\ T_M\right)}{\partial y} = \frac{\partial}{\partial x}\left(k_M \frac{\partial T_M}{\partial x}\right) + \frac{\partial}{\partial y}\left(k_M \frac{\partial T_M}{\partial y}\right) + \frac{\partial}{\partial x}\left(\rho_M D(C_{p_v} - C_{p_g})\frac{\partial W}{\partial x} T_M\right) + \frac{\partial}{\partial y}\left(\rho_M D(C_{p_v} - C_{p_g})\frac{\partial W}{\partial y} T_M\right) \tag{8}$$

$$\frac{\partial}{\partial t}(\rho_M\ W) + \frac{\partial}{\partial x}(\rho_M\ U_M\ W) + \frac{\partial}{\partial y}(\rho_M\ V_M\ W) = \frac{\partial}{\partial x}\left(\rho_M\ D \frac{\partial W}{\partial x}\right) \frac{\partial}{\partial y}\left(\rho_M\ D \frac{\partial W}{\partial y}\right) \tag{9}$$

Equations (5), (6), (7), and (8) are the continuity, x-momentum conservation, y-momentum conservation, and energy conservation equations, respectively. Equation (9) represents mass conservation for the gas. The thermophysical and transport properties were calculated as functions of the local temperature, pressure and mixture composition [13].

A. Conditions Prescribed at the Liquid-Mixture Interface

At the interface, flow fields must be coupled appropriately by applying jump conditions that relate the variables in each side of the interface. The interface conditions are implemented using two rows of zero-width control volumes.

A normal force balance is enforced using (10):

$$(\hat{n} \cdot \boldsymbol{\tau})_L \cdot \hat{n} = -(\hat{n} \cdot \boldsymbol{\tau})_M \cdot \hat{n} \tag{10}$$

where $\boldsymbol{\tau}$ is the stress tensor, $\hat{n}$ is the local normal unit vector to the interface. For the present work, the surface tension effects are neglected.

A tangential force balance is enforced using (11):

$$(\hat{n} \cdot \boldsymbol{\tau})_L \cdot \hat{s} = (\hat{n} \cdot \boldsymbol{\tau})_M \cdot \hat{s} \tag{11}$$

where $\hat{s}$ is the local tangential unit vector to the interface.

Conservation of mass and interfacial mass flow due to condensation are prescribed using (12):

$$\dot{m}_{L,i} = \dot{m}_{M,i} = \dot{m}_{\text{cond}} \tag{12}$$

The interface condensation rate is calculated using (13):

$$\dot{m}_{\text{cond}} = \frac{A_i}{h_{fg}}\left(-k_L \left.\frac{\partial T_L}{\partial n}\right|_i + k_M \left.\frac{\partial T_M}{\partial n}\right|_i\right) \tag{13}$$

Equations (14) and (15) are the continuity of tangential velocity and temperature, respectively.

$$\overrightarrow{(V_t)}_{L,i} = \overrightarrow{(V_t)}_{M,i} \tag{14}$$

$$T_L = T_M = T_{sat} \tag{15}$$

Impermeability to gas at the interface is prescribed applying (16):

$$\dot{m}_{M,i} W_i - (\rho_M D)_i A_i \left.\frac{\partial W}{\partial n}\right|_i = 0 \tag{16}$$

where A_i is the local interfacial area. Equation (17) is a final closure condition for pressure in the mixture at the interface.

$$\left.\frac{\partial P}{\partial n}\right|_{M,i} = 0 \tag{17}$$

B. Boundary Conditions

At the inlet (bottom) for the flow going in, uniform profiles of $T_{\rm in}$, $P_{\rm in}$, and $W_{\rm in}$ are specified. Saturation conditions are assumed. For the flow going out in the liquid and part of the mixture, fully developed boundary conditions are applied.

At the outlet (top), fully developed boundary conditions are prescribed. For reasons described later, a film thickness of 1×10^{-7} m is specified at the top. A uniform liquid inlet velocity of 1×10^{-7} m/s is prescribed for the liquid inlet velocity at the top. A reference pressure $P_{\rm ref}$, relative to $P_{\rm in}$ is specified at the outlet in order to obtain a given $\Delta P = P_{\rm in} - P_{\rm ref}$.

At the wall ($y = 0$), no slip boundary conditions are imposed as shown in (18).

$$U_{\scriptscriptstyle L} = 0 \quad , \quad V_{\scriptscriptstyle L} = 0 \tag{18}$$

The wall temperature is constant and uniform along the cooled section (L_2). For the two bottom and top sections (L_1 and L_3), adiabatic wall is assumed as shown in (19).

$$\begin{aligned} T_{\scriptscriptstyle L} &= T_{\rm wall} \qquad \text{for} \quad 0 \le x \le L_2 \\ q''_{\rm wall} &= 0 \qquad \text{for} \quad -L_1 \le x < 0 \text{ and } L_2 < x \le L_3 \end{aligned} \tag{19}$$

At the centre line ($y = H$), symmetry is prescribed using (20).

$$V_{\scriptscriptstyle M} = 0 \quad , \quad \frac{\partial U_{\scriptscriptstyle M}}{\partial y} = \frac{\partial T_{\scriptscriptstyle M}}{\partial y} = \frac{\partial W}{\partial y} = 0 \tag{20}$$

C. Algorithm for Moving the Mesh

In this work the location of the interface that is separating the phases is part of the solution. At each time step, the solution fields are computed using a fixed mesh. At the end of each time step, the location of the interface is updated. This update is based on an integral liquid mass balance (ILMB) equation at all axial locations where there are nodes.

A mass balance is made on each column of control volumes in the liquid region. This mass balance is written as (21).

$$\int_0^{\delta_w} \rho_{\scriptscriptstyle L} U_w \, dy + \dot{m}_{cond} = \int_0^{\delta_e} \rho_{\scriptscriptstyle L} U_e \, dy \tag{21}$$

where δ_w and δ_e are the film thicknesses on the left and right sides of the particular column of control volumes in the liquid phase. Equation (21) therefore leads to a connection between δ_w and δ_e and can be applied, starting at the inlet, to determine the film thickness all along the domain. At the inlet, the film thickness is zero. In practice, because we use a structured grid, a zero height of liquid at the interface is not used. Instead, the position of the node on the interface at the inlet is fixed at a y distance of 10^{-7} m from the wall. This helps generating the grid in the liquid region from the beginning of the solution. Numerical integration of the (21) is done with the help of face velocities and, by applying a forward marching scheme, results the value of δ_e for all the nodal locations along the x-direction.

III. Numerical Solution Method

A structured, non-orthogonal grid is used to discretise the domain. The grid generation uses transfinite interpolation and permits splitting the domain into different panels in the coordinate directions, as described in [14]. In this work, the grid was generated using two panels in the y direction: one for each phase region and three panels in the x direction: one for each section. The starting mesh for a calculation was obtained in two ways. In some cases, an initial rectangular mesh with a liquid height of 10^{-7} m was used. In other cases, the mesh from a previously converged calculation for different boundary conditions was used as the initial mesh. In all cases the mesh is moved at the end of each time step as previously described.

In the computational mesh the x-direction length is divided into N_x uniformly spaced control volumes, excluding boundary nodes. In the y-direction, the liquid region has $N_{y,L}$ uniformly spaced control volumes and the mixture has $N_{y,M}$ non-uniformly spaced control volumes. Grid expansion factors were used in the mixture region to obtain better resolution near the interface.

The governing partial differential equations for U, V, T, P and W were discretised to get the coupled algebraic equation set using a finite volume method [15]. A co-located variable storage scheme is applied in this work. The pressure-velocity coupling is treated by using an approach based on the work of Rhie and Chow [16]. It is similar to the approach described by Yu *et al.* [17] and Vakilipour and Ormiston [18].

An in-house computer code implements this solution approach. The code was tested by solving several non-condensing two-phase laminar flow cases. For example, a horizontal stratified gas-liquid flow in a channel and falling film on a vertical plate were solved and the results compared well with the literature. In addition, results that match the Nusselt solution for pure vapour condensation were successfully produced by the code. The code results were also validated by comparing with the previous available works for co-current condensation [19].

Grid independence tests were carried out based on the film thickness for all cases that are presented in this paper. The range of values considered was as follows: $75 \le N_x \le 250$ with $1.0 \le r_x \le 1.02$, $20 \le N_{y,L} \le 40$, and $20 \le N_{y,M} \le 100$ with $1.0 \le r_{y,M} \le 1.1$. A grid with N_x= 175 with r_x= 1.00, $N_{y,L}$= 20, $N_{y,M}$= 80 with $r_{y,M}$= 1.1 had normalized maximum difference of film thickness of less than 1.07 % compared to a coarser mesh. Therefore, this grid was used for the results presented in this article.

At the beginning of cooled section, there is a sudden jump in the liquid thickness (beginning of liquid film build up). Therefore, the first control volumes of the cooled section are extremely skewed. Having skewed control volumes results in seeing a small bump in the interface location at this region. To avoid this, an extremely fine grid is needed at the beginning of cooled section. However, the application of really fine grids increases the cost of computation significantly. Typical runs for the mentioned grid size takes about 20 days to finish with the application of 24 computation cores. The cost of computation originates from the matrix of coefficients which is highly

ill-conditioned with eigenvalue range of 1.0E-14 to 1.0E+04 and the condition number of 1.0E+07. Therefore, only a parallel direct solver (superlu-dist) with the PETSc parallel solver [20] could be used to solve the coupled algebraic equation set. A suitable iterative solver could not be made to work.

IV. Results and Discussion

Results were obtained for a steam-air mixture at relative inlet pressures of $\Delta P = 4$ Pa and $\Delta P = 7$ Pa for two channels with different lengths: short and long. Other pressures and lengths in the laminar regime are possible. Trends discussed here will be similar under other conditions.

The half height of the channel was specified to be $H = 2.5$ mm and the plate lengths were $L = 250$ mm (short channel) and $L = 600$ mm (long channel). For the short channel L_1 and L_3 were set to 100 mm and 120 mm and for the long channel, they were set to 250 mm and 100 mm, respectively. The present model was run for cases with $W_{\rm in} = 0.0$ and 0.001 and the inlet-to-wall temperature difference of $\Delta T = 1$ K.

The sample results presented in this paper include the profiles of velocity and gas mass fraction as well as the film thickness for the mentioned cases. Due to the build up of the film and significant variations near the beginning of the cooled section, transverse profiles of axial velocity and gas mass fraction are presented far from this region. Important details are found by plotting transverse profiles of axial velocity close to the interface which includes the liquid and gas velocities. Additional insights are drawn from examining the inlet pressure variation for a specific length of the channel.

Fig. 2 shows the axial variation of the liquid film thickness for all cases with $\Delta P = 4$ Pa and $\Delta P = 7$ Pa for the short and long channel, respectively. The film thickness did not change as the gas mass fraction at the inlet decreases from 0.001 to 0. In addition, this figure shows that the non-dimensional value of film thickness with respect to $x^\star$ is the same for both channel lengths. As discussed before, there is a small bump in the film thickness at $x^\star = 0.16$ and $x^\star = 0.67$ for the short and long channels, respectively. This is due to the skewness of the grid because of the sudden change of film thickness at that spot. Applying finer grid at the beginning of cooled section may resolve this issue. However, this leads to prohibitive computational cost. Also, the small bump does not have an impact on the interface height along the channel.

The axial velocity profiles in three different stations are given in Fig. 3 for $W_{\rm in} = 0.001$ using the dimensionless coordinate η defined by (22). The relative inlet pressure was set to 4 Pa and 7 Pa for the short and long channel, respectively.

$$\begin{aligned} \eta &= y/\delta \qquad \text{for} \quad 0 \le y \le \delta \\ \eta &= (y-\delta)/(H-\delta)+1 \qquad \text{for} \quad \delta \le y \le H \end{aligned} \tag{22}$$

At the inlet, the velocity profiles are similar to the fully-developed channel velocity profiles for both lengths. The cooled section inlet Reynolds numbers based on average gas phase velocity and channel half width are $\mathrm{Re}_{\rm in,c} = 1228.6$ and

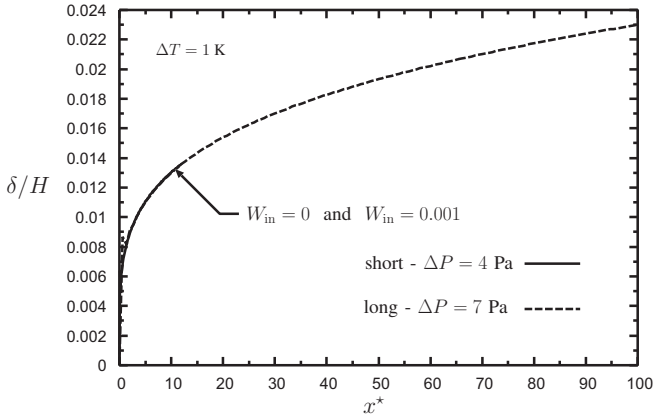

Fig. 2 Film thickness

$\mathrm{Re}_{\rm in,c} = 1375.3$ for the short and long channel, respectively. Due to the condensation, vapour has been removed from the gas-vapour mixture toward the outlet. Therefore, the velocities decrease and the higher length of cooled section for the long channel leads to higher reduction of the velocity values. Negative velocity corresponds to upward flow in the mixture region. There are positive velocities in the liquid region and close to the interface in the mixture region which are shown next.

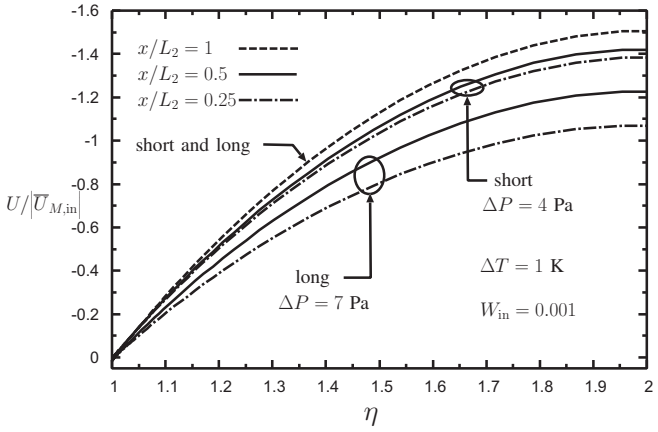

Fig. 3 Velocity profiles

Fig. 4 shows the velocity profiles in the liquid region and close to the interface in the mixture region for the same stations and cases as in Fig. 3. The profiles are plotted versus y/H instead of η in order to clearly show the velocity profiles in the liquid and mixture near the interface for different film thicknesses. The liquid mixture interface coincides with the sudden change in slope of the velocity profiles. These profiles indicate that there is a sudden small decrease in the magnitude of the liquid velocity at the interface (*i.e.*, $\frac{\partial U_L}{\partial y} < 0$ at the interface). Note the region of positive mixture velocity and the change of sign in the mixture velocity profiles. The sign change point will be referred to as the boundary point between the downflow and upflow. Positive velocities in the mixture region correspond to the flow going out from the bottom of the domain. Shear force at the interface pulls the mixture

down and causes downward flow in the mixture. This positive velocity region in the mixture becomes smaller toward the outlet (top of the domain) and finally at the outlet there is no positive velocity. Basically, inlet-to-wall temperature difference, inlet pressure and inlet gas mass fraction are the key parameters that determine the place of the boundary point. The point could move to the liquid region for small film thickness and high mixture inlet velocity. In these cases, the gravity force may not be larger than shear force at the interface and liquid starts flowing upward.

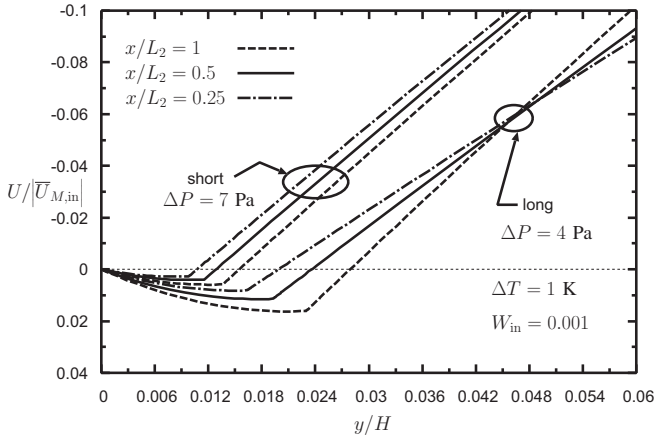

Fig. 4 Velocity profiles close to the interface

Gas mass fraction profiles are presented in Fig. 5 for the cases with $W_{\text{in}} = 0.001$ and $\Delta P = 7$ Pa. As expected, longer length of condensation results in higher gas mass fraction because of the greater vapour removal from the mixture. It is shown that highest gas mass fraction values occur at the interface for all cases. The gas mass fraction does not change significantly along the cooled section. Low condensation rate due to the small inlet-wall-temperature difference and the downward flow in the mixture region near the interface could be the possible reasons for the small gas mass fraction variation.

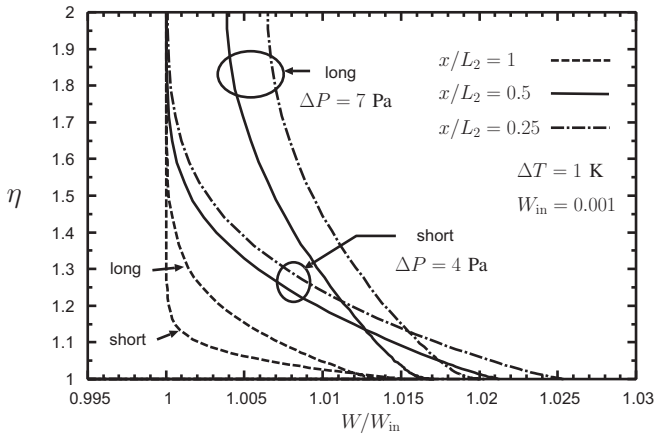

Fig. 5 Gas mass fraction profiles

Inlet relative pressure value is a key parameter to control the amount of mass flow rate going in the channel. Small inlet relative pressure does not bring enough mass for the condensation process. Thus, the condensation driving force pulls the mass from the outlet (top) of the channel. In these cases, the condensation rate is mainly governed by the length of the cooled section, inlet gas mass fraction and inlet-to-wall temperature difference. Fig. 6 shows the case where the inlet relative pressure was not high enough to force the mass to exit the channel from the top. Compared to the previous cases, the inlet relative pressure was reduced to $\Delta P = 4$ Pa for the long channel. As can be seen, condensation driving force starts pulling vapour from the top. Thus, the mixture velocity near the beginning of the cooled section ($x/L_2 = 0$) is positive. This means that vapour is coming from both top and bottom of the channel. The outflow is at the bottom which contains liquid and a small amount of vapour. The vapour downflow is caused by the shear force at the interface.

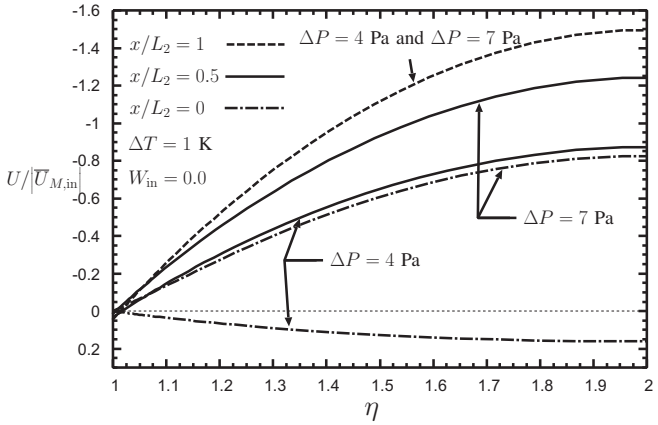

Fig. 6 Velocity profiles for different inlet pressures

V. Summary and Conclusions

A numerical model was presented for steady, laminar reflux condensation from vapour-gas mixtures based on the complete elliptic set of equations. A sharp interface tracking method and a fully coupled solution approach were used.

Numerical results were obtained for steam-air mixture flow in two different channel lengths for two different relative inlet pressures. Pure vapour and gas-vapour mixture with gas mass fraction of 0.001 with fixed inlet-to-wall temperature difference were investigated. Sample results were given for the axial variation of the film thickness as well as selected axial velocity profiles and gas mass fraction.

Velocity profiles in the mixture demonstrated that there is a boundary point between the upflow and downflow. The downflow region gets smaller toward the outlet. Also, it was shown that for the channel with short cooled section, this region is smaller.

For the cases with the presence of gas, the highest gas mass fraction values were observed at the interface due to the vapour removal caused by condensation.

The effect of relative pressure value was discussed. It was shown that for avoiding mass coming in from the outlet (top of the domain), the inlet relative pressure should be sufficiently

large. Otherwise, the condensation driving force starts pulling mass in from the outlet.

ACKNOWLEDGMENT

The financial support of the University of Manitoba for a Graduate Fellowship to the first author (FH) and of NSERC for a Discovery Grant to the second author (SO) are gratefully acknowledged. In addition, the authors sincerely appreciate the invaluable high performance computing technical help of Hossein Pourreza and Grigory Shamov. The authors also acknowledge the support of Compute Canada and WestGrid.

APPENDIX A
NOMENCLATURE

A	area, $[m^2]$
C_p	specific heat, $[J/kg \cdot K]$
D	diffusion coefficient, $[m^2/s]$
g	acceleration due to gravity, $[m/s^2]$
h_{fg}	latent heat of vapourisation, [J/kg]
H	channel half width,[m]
L	plate length,[m]
k	thermal conductivity, $[W/m \cdot K]$
$\dot{m}$	mass flow rate, $[kg/s]$
n	normal direction, [m]
$\hat{n}$	normal unit vector
$N_{y,L}$	number of nodes along the y direction, liquid region
$N_{y,M}$	number of nodes along the y direction, mixture region
N_x	number of nodes along the x-direction
P	pressure, $[N/m^2]$
ΔP	relative pressure $(P_{\rm in} - P_{\rm ref})$, $[N/m^2]$
$\mathrm{Re}_{\rm in}$	inlet Reynolds number, $(4\rho_{\rm in}\overline{U}_{M,{\rm in}}H)/\mu_{\rm in}$
r_x	expansion factor in x direction
$r_{y,M}$	expansion factor in y direction, mixture region
$\hat{s}$	tangent unit vector
T	temperature, $[K]$
t	time, $[s]$
U, V	velocities in the Cartesian x and y directions, $[m/s]$
$\overline{U}$	average velocity in x direction, $[m/s]$
$\overrightarrow{V_t}$	tangential velocity vector, $[m/s]$
W	gas mass fraction, $\frac{m_g}{m_{tot}}$
$x^\star$	dimensionless length, x/H
x, y	Cartesian coordinate directions, [m]

Greek Letters

η	dimensionless y-direction coordinate
δ	thickness of the condensate layer, [m]
δ^*	dimensionless film thickness (=δ/H)
μ	dynamic viscosity, $[N \cdot s/m^2]$
$\boldsymbol{\tau}$	stress tensor, $[N/m^2]$
ρ	density, $[kg/m^3]$

Subscripts

c	referring to the cooled section
cond	referring to the condensate
e	referring to the east
g	referring to the gas
i	referring to the liquid-mixture interface
in	referring to the inlet
L	referring to liquid
M	referring to mixture
ref	referring to reference
sat	referring to saturation condition
v	referring to vapour
w	referring to the west
wall	referring to the wall

REFERENCES

[1] J. Palen and Z. Yang, "Reflux condensation flooding prediction: Review of current status," *Chemical Engineering Research and Design*, vol. 79, no. A4, pp. 463–469, May 2001.

[2] Y. Moon, H. Park, Y. Bang, U. N. R. C. O. of Nuclear Regulatory Research, H. Kisurwŏn, H. Yŏnoguso, and H. Kisurwŏn, *Assessment of RELAP5/MOD3. 2 for Reflux Condensation Experiment*. Office of Nuclear Regulatory Research, US Nuclear Regulatory Commission, 2000.

[3] Y. Utanohara and M. Murase, "Numerical analysis of steam-air behavior in a pressurizer during reflux cooling," *Nucl. Eng. Des.*, vol. 240, no. 12, pp. 3930–3941, Dec. 2010.

[4] S. Chen, J. Reed, and C. Tien, "Reflux condensation in a two-phase closed thermosyphon," *International Journal of Heat and Mass Transfer*, vol. 27, no. 9, pp. 1587 – 1594, 1984. (Online). Available: http://www.sciencedirect.com/science/article/pii/0017931084902710

[5] R. Seban and J. Hodgson, "Laminar film condensation in a tube with upward vapor flow," *International Journal of Heat and Mass Transfer*, vol. 25, no. 9, pp. 1291 – 1300, 1982. (Online). Available: http://www.sciencedirect.com/science/article/pii/0017931082901235

[6] R. Girard and J. S. Chang, "Reflux condensation phenomena in single vertical tubes," *Int. J. Heat Mass Trans.*, vol. 35, no. 9, pp. 2203–2218, 1992.

[7] G. Chou and J. Chen, "Heat transfer characteristics of reflux condensation phenomena in a single vertical tube," *Nucl. Sci. Eng.*, vol. 127, no. 2, pp. 220–229, Oct. 1997.

[8] ——, "A general modeling for heat transfer during reflux condensation inside vertical tubes surrounded by isothermal fluid," *International Journal of Heat and Mass Transfer*, vol. 42, no. 12, pp. 2299–2311, June 1999.

[9] Y. Pan, "Condensation characteristics inside a vertical tube considering the presence of mass transfer, vapor velocity and interfacial shear," *International Journal of Heat and Mass Transfer*, vol. 44, no. 23, pp. 4475 – 4482, 2001. (Online). Available: http://www.sciencedirect.com/science/article/pii/S0017931001000874

[10] S. Fiedler and H. Auracher, "Experimental and theoretical investigation of reflux condensation in an inclinded small diameter tube," *Int. J. Heat Mass Trans.*, vol. 47, pp. 4031–4034, 2004.

[11] Y. Liao, S. Guentay, D. Suckow, and A. Dehbi, "Reflux condensation of flowing vapor and non-condensable gases counter-current to laminar liquid film in a vertical tube," *Nucl. Eng. Des.*, vol. 239, no. 11, pp. 2409–2416, Nov. 2009.

[12] V. K. Liao, Y., "A generalized diffusion layer model for condensation of vapor with noncondensable gases," *ASME Journal of Heat Transfer 129, 988-994*, 2007.

[13] F. Hassaninejadfarahani, M. Guyot, and S. Ormiston, "Numerical analysis of mixed-convection laminar film condensation from high air mass fraction steamair mixtures in vertical tubes," *International Journal of Heat and Mass Transfer*, vol. 78, pp. 170 – 180, 2014. (Online). Available: http://www.sciencedirect.com/science/article/pii/S0017931014005195

[14] Y. Q. Wang, L. A. Penner, and S. J. Ormiston, "Analysis of laminar forced convection of air for crossflow in banks of staggered tubes," *Numerical Heat Transfer, Part A (Applications)*, vol. 38, no. 8, pp. 819–845, 2000.

[15] S. V. Patankar, *Numerical Heat Transfer and Fluid Flow*. Washington: Hemisphere, 1980.

[16] C. M. Rhie and W. L. Chow, "Numerical Study of the Turbulent Flow Past an Airfoil with Trailing Edge Separation," *AIAA J.*, vol. 21, no. 11, pp. 1525–1532, 1983.

[17] B. Yu, Y. Kawaguchi, W. Tao, and H. Ozoe, "Checkerboard pressure predictions due to the underrelaxation factor and time step size for a nonstaggered grid with momentum interpolation method," vol. 41, no. 1, pp. 85–94, 2002.
[18] S. Vakilipour and S. Ormiston, "A coupled pressure-based co-located finite-volume solution method for natural-convection flows," *Numerical Heat Transfer, Part B (Fundamentals)*, vol. 61, pp. 91–115, 2012.
[19] F. Hassaninejadfarahani and S. Ormiston, "Fully coupled elliptic numerical model for film condensation from vapour-gas mixtures in vertical parallel plate channels," in *Proceedings of the ASME 2014 International Mechanical Engineering Congress and Exposition*, vol. 8A, Montreal, Canada, 2014.
[20] S. Balay, S. Abhyankar, M. F. Adams, J. Brown, P. Brune, K. Buschelman, V. Eijkhout, W. D. Gropp, D. Kaushik, M. G. Knepley, L. C. McInnes, K. Rupp, B. F. Smith, and H. Zhang, "PETSc users manual," Argonne National Laboratory, Tech. Rep. ANL-95/11 - Revision 3.5, 2014. (Online). Available: http://www.mcs.anl.gov/petsc

Foad Hassaninejadfarahani is Ph.D. candidate at the University of Manitoba, Canada. Foad recieved his M.Sc. and B.Sc. in Mechanical Engineering at the Iran University of Science and Technology and K.N.Toosi University of Technology, Iran. His main research area is computational fluid dynamics methods development with applications in heat and mass transfer of two-phase flows and fluid-structure interaction.

Scott Ormiston is a professor in the Department of Mechanical Engineering at the University of Manitoba. He received his Ph.D. from the University of Waterloo in Canada and has 34 years of experience in numerical modelling of heat transfer and fluid flow. His main research area is computational fluid dynamics methods development with applications in heat and mass transfer of two-phase flows with phase change.